8th Asia Conference on Earthquake Engineering
Taipei, Taiwan ■ November 9-11, 2022

Analysis and Test Plan for a Three-Story Steel BRBF with a Sliding Slab to Reduce Seismic Lateral Force in Shake Table Tests

Chung-Che Chou[1], Alvaro Córdova[2], Huang-Zuo Lin[3], Jian-Ming Chen[3], Yen-Hsun Chou[4], Shu-Hsien Chao[5], Shih-Ho Chao[6], Georgios Tsampras[7], China-Ming Uang[8], Hsin-Yang Chung[9], Hsuan-Teh Hu[10], Chin-Hsiung Loh[11]

1. Director General, National Center for Research on Earthquake Engineering, Taipei, Taiwan
Professor, National Taiwan University, Taipei, Taiwan
2. Ph.D. student, National Taiwan University, Taipei, Taiwan
3. Master student, National Taiwan University, Taipei, Taiwan
4. Master student, National Cheng Kung University, Tainan, Taiwan
5. Research Fellow, National Center for Research on Earthquake Engineering, Taipei, Taiwan
6. Professor, University of Texas, Arlington, USA
7. Assistant Professor, University of California, San Diego, USA
8. Professor, University of California, San Diego, USA
9. Associate Professor, National Cheng Kung University, Tainan, Taiwan
10. Professor, National Cheng Kung University, Tainan, Taiwan
11. Adjunct Professor, National Taiwan University, Taipei, Taiwan

Email: cechou@ntu.edu.tw

ABSTRACT

A new system for reducing the seismic force of traditional steel buildings is investigated through a collaboration work between the US and Taiwan. It involves a set of horizontal energy dissipating devices, working with the traditional Lateral Force Resisting System to speed up the on-site construction and enhance the seismic performance of steel buildings. This is achieved by allowing the slab to slide with respect to the steel frame, activating a horizontal energy dissipation device (i.e., horizontal buckling-restrained brace, HBRB) connected to the slab and beam to provide resistance. A design procedure based on ASCE/SEI 7-16 (2016) was validated through nonlinear time history analyses, conducted on a three-story steel Buckling-Restrained Braced Frame (BRBF) with different sets of horizontal devices. The analysis showed that by using this design procedure, the deformation of the horizontal device could limit to an axial strain of 4.5% during a strongest near-fault earthquake motion, and the peak frame roof drift could be about 1%. A full-scale, three-story steel frame with a sliding slab linked to a HBRB at each floor will be tested by using a shake table at NCREE to validate the proposed design procedure.

Keywords: Horizontal buckling-restrained brace, sliding slab, Near-fault motion, Shake table test, Time history analysis.

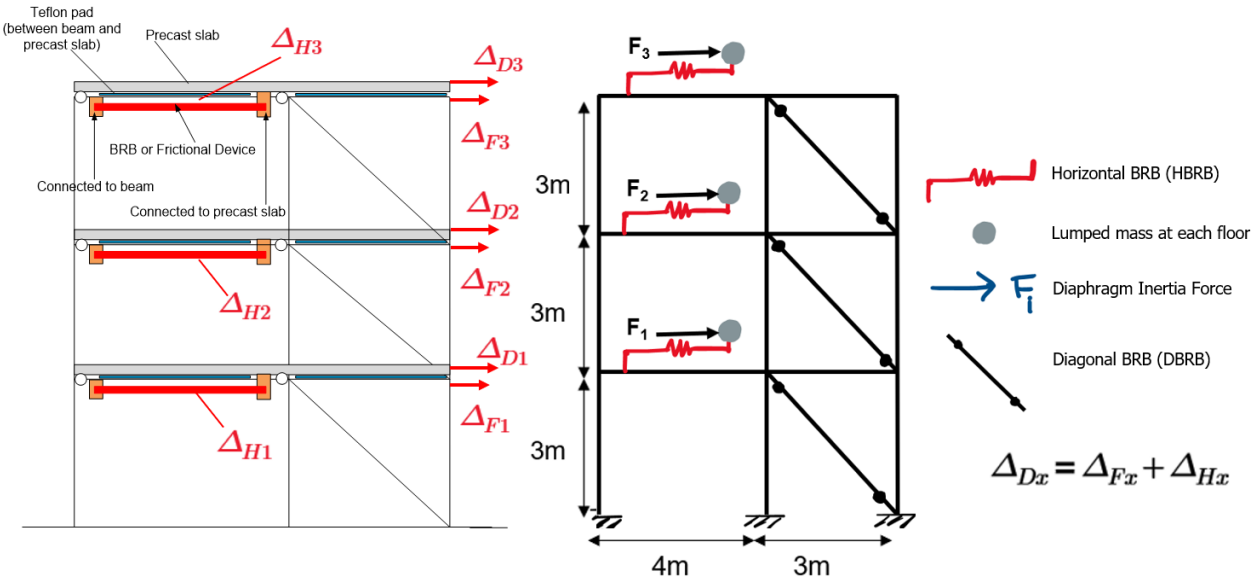
INTRODUCTION

A new system is investigated in this work by introducing a horizontal energy dissipation device between the slab and beams in the Lateral Force Resisting System (LFRS); no shear studs are used between the steel beam and slab as in the conventional steel frame system. The slab slides with respect to the beam, allowing energy dissipation devices to provide horizontal resistance (called “New System” in this work) in addition

to the conventional moment-resisting system that accounts on the ductility of vertical frame members. The new system aims to decrease forces and drifts developed in the LFRS, and total accelerations developed in the floors. Among a variety of ductile devices, a sandwich buckling-restrained brace (SBRB) that was verified to provide stable hysteretic response and deformation capacity (Chou and Chen 2010, Chou et al. 2012, 2016) will be used between the slab and beams in this new steel frame. Currently, there are no guidelines to size these horizontal energy dissipating members for steel buildings with slabs that are allowed to slide relative to a steel frame. Tsampras et al. (2022) proposed a step-by-step method for the design of connections that limit the forces transferred from conventional gravity load resisting systems to LFRS with flexural yielding base mechanism (e.g. structural walls) or rocking base mechanism (e.g., steel self-centering concentrically braced frames or rocking post-tensioned structural walls in Tsampras 2016, Tsampras et al., 2016, Zhang et al., 2018, Tsampras et al. 2022). This conference paper proposes a procedure to calculate initial design forces for the Horizontal BRBs (HBRB) that connect the sliding slab with the LFRS in a three-story steel buckling-restrained braced frame (BRBF) based on ASCE/SEI 7-16 section 12.10.1 (2016). The building was modeled as a 2D frame using nonlinear time history analyses (NLTH) in the PISA3D computer program. A full-scale, three-story steel frame with a sliding slab connected to HBRBs at each floor will be tested by using a shake table at Tainan Lab, NCREE to validate the proposed design procedure in November 2022.

THREE-STORY STEEL PROTOTYPE FRAME

Fig. 1 shows a prototype, which is a steel dual system composed of a Special Moment Frame (SMF, left bay) and a BRBF (right bay). All columns are steel built-up box columns that satisfy the moderately ductile member requirement in AISC 341-16 (2016); similar columns, tested by Chou and Chen (2020) and Chou et al. (2022), showed good cyclic performance at 4% drift. All three HBRBs are sandwiched buckling-restrained braces, designed based on a design procedure in Chou and Chen (2010). The HBRBs were modeled using a truss element and the steel core properties were based on kinematic hardening material parameters in Chou et al. (2012). All masses were lumped at one end of the HBRBs for inelastic time history analysis of the frame, and the damping ratio was 2%. In Fig. 1, a symbol Δ_{Hx} is the HBRB displacement at floor x; Δ_{Fx} is the frame displacement at floor x, and Δ_{Dx} is the diaphragm displacement at floor x.



(a) Original building system (b) Structural model

Figure 1. Three-story prototype with BRBF, SMF and sliding slabs.

Proposed Design Procedure

The section 12.10.1 of ASCE/SEI 7-16 (2016) has a procedure to compute diaphragm design forces for buildings. This force level represents the absolute maximum floor acceleration during a given earthquake, thus representing an acceleration envelope. For this procedure, it is first required to obtain the base shear from the Equivalent Lateral Force (ELF) procedure, and then, given the floor masse w_x, and height h_x, to compute floor force F_x [Eq. (1)]. A parameter, k, accounts for higher mode contribution in upper floors (Lopez and Cruz 1996). Eq. (2) is used to determine the diaphragm design forces, where the numerator is F_x in Eq. (1). In addition, there is a lower bound, $0.2S_{DS}I_e w_{px}$, and an upper bound, $0.4S_{DS}I_e w_{px}$, which represent 0.5 and 1.0 times the Peak Ground Acceleration (PGA), respectively (where S_{DS} is the design spectral acceleration for short periods and I_e is the importance factor). The code recommends that floor acceleration should exceed at least 0.5PGA. These limits are independent of the system ductility R and Ω_o because the diaphragm detailing usually doesn't depend on the selected structural system. Eq. (2) provides a larger set of forces than Eq. (1), more significant in lower floors resulting in a steeper slope of the floor force distribution. For example, for same floor masses, w_x, and heights, h_x, in all three floors, Eq. (1) results in force ratios of 1, 2, and 3, and Eq. (2) results in force ratios of 1, 1.25, and 1.5. Although this design method still considers the vertical ductility of the traditional system (i.e., the horizontal ductility of the new system is not considered), it was shown to provide an acceptable initial design for the horizontal devices.

While F_{px} forces at each floor are obtained from Eq. (2), the HBRB core area at each floor can be computed based on LRFD procedure. For this model, the calculated parameters are as follows: $w_x = w_{px} =$ 327 kN, $h_x = 3$ m (for all floors), $k = 1.0$, $C_s = 0.242$ g for Tainan and the base shear is $V = 237.4$ kN. Forces from ELF procedure are: $F_1 = 39.6$ kN, $F_2 = 79.1$ kN and $F_3 = 118.7$ kN. Diaphragm forces for the DBE level are: $F_{p1} = 79.1$ kN, $F_{p2} = 98.9$ kN, $F_{p3} = 110.88$ kN. Diaphragm forces for the maximum-considered earthquake (MCE) level are: $F_{p1} = 118.65$ kN, $F_{p2} = 148.35$ kN, $F_{p3} = 166.32$ kN. The HBRB core can be determined based on $\phi P_n > P_u$, where $P_n = A_{sc}F_y$, A_{sc} and F_y are the HBRB steel core area and the yield strength, respectively, and $\phi = 1.0$. Since the diaphragm force, F_{px}, is transferred directly to the HBRB, replacing P_u in the later equation by F_{px} at the MCE level. The resulting core areas are 163 mm^2, 204 mm^2 and 228 mm^2 for 2nd, 3rd and roof floor, respectively, as listed in Table 2. Two HBRBs per floor are considered to avoid force eccentricities.

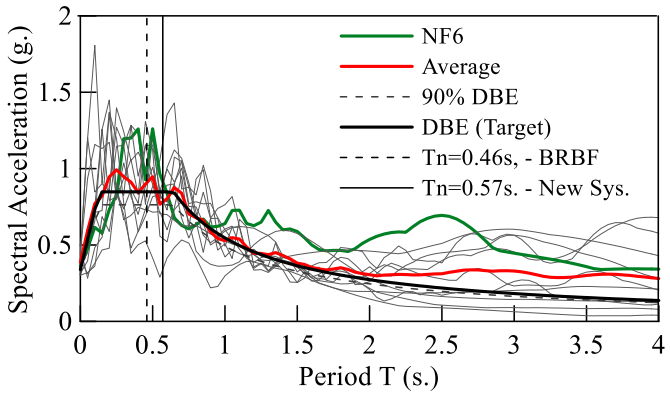
$$F_x = \frac{w_x \cdot h_x^{\,k}}{\sum_{i=1}^{n}\left(w_i \cdot h_i^{\,k}\right)} \cdot V \quad (1)$$

$$F_{px} = \frac{\sum_{i=x}^{n} F_i}{\sum_{i=x}^{n} w_i} w_{px} \quad (2)$$

ANALYSIS AND RESULTS

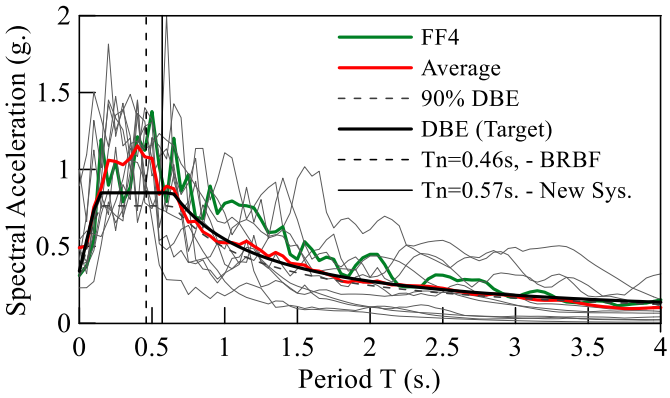
Fig. 2 shows eleven near-fault motions and eleven far-field motions, scaled to match the Design Based Earthquake (DBE) for the three-story prototype frame based on Lin and Chou (2022). The two green motions NF6 and FF4 are the most representative to the system, as shown in Fig. 2(a) and (b). The NF6 motion was used as an example for the illustration of the prototype under the near-fault earthquake motion.

-NF1 Chi-Chi-CHY101-E
-NF2 Chi-Chi-TCU029-E
-NF3 Chi-Chi-TCU029-W
-NF4 Chi-Chi-TCU031-E
-NF5 Chi-Chi TCU053-E
-NF6 Chi-Chi-TCU068-EW
-NF7 El Centro-#6-230
-NF8 Landers LCN-260
-NF9 Northridge-01 Sta-360
-NF10 Kobe-KJMA-000
-NF11 Christchurch-PRP-W



(a) Eleven near-fault motions

-FF1 Chi-Chi - TCU095NS
-FF2 Chi-Chi - CHY015NS
-FF3 Chi-Chi - CHY015EW
-FF4 Jiasian - CHY099NS
-FF5 Wutai - CHY099NS
-FF6 Meinong - CHY133NS
-FF7 Whittire Narrows - ALT360
-FF8 Northridge - CNP196
-FF9 Landers - IND090
-FF10 Kobe - ABN090
-FF11 Christchurch - RHSCS04W



(b) Eleven far-field motions

Figure 2. Earthquake motions for time history analysis of the frame.

The two controlling parameters for all analyses are that (1) the HBRBs shouldn't exceed an axial strain of 4.5% and (2) HBRB strain along the building height should be uniformly distributed. An effort was made to optimize the design based on these two constraints. This was achieved by trying different sets of HBRBs, called "Cases" as listed in Table 1. Peak strains of HBRB at each floor in five cases are plotted in Fig. 3. The best case (i.e., labeled by Case 3* in this work), based on these two controlling parameters, was very close to results based on Eq. (2) at the MCE level as design forces (5% difference). Fig. 3 shows a summary of the results where the horizontal axis represents cases with different sets of HBRBs (five cases are shown). HBRBs in case 1 were designed based on the lowest forces, thus having the smallest BRB cores; HBRBs in case 5 were designed based on the largest forces, thus having the largest BRB cores. The HBRBs exceeded the deformation capacity in cases 1 and 2, and the HBRBs in cases 4 and 5 did not fully develop the maximum deformation capacity. Case 3* shown below is the result of using Eq. (2) for design; the HBRB showed not only a peak strain of 4.3% at the roof (very close to the deformation target of HBRB), but also a more uniform strain distribution along the building height compared to other cases (see Tables 1 and 2). Table 2 shows the maximum strains of HBRBs and diagonal BRBs (DBRB) at each floor; Fig. 3 also shows the maximum force of DBRBs (as shown by $P/P_y > 1$), which increases with the case number since the force demand is larger as the HBRB core area increases (higher P_y of HBRB).

Table 1: Core yield forces (P_y), areas (A_{sc}) and peak strains for five HBRB cases using NF6 motion.

	CASE 1			CASE 2			CASE 3*			CASE 4			CASE 5		
Floor	HBRB Py (kN)	HBRB Asc (mm^2)	HBRB Max. Strain (%)	HBRB Py (kN)	HBRB Asc (mm^2)	HBRB Max. Strain (%)	HBRB Py (kN)	HBRB Asc (mm^2)	HBRB Max. Strain (%)	HBRB Py (kN)	HBRB Asc (mm^2)	HBRB Max. Strain (%)	HBRB Py (kN)	HBRB Asc (mm^2)	HBRB Max. Strain (%)
Roof	60	165	7.5%	40	110	11.5%	83	228	**4.3%**	91	250	2.8%	102	280	1.3%
3rd	40	110	10.5%	33	90	13.2%	74	204	1.3%	82	225	0.6%	91	250	0.2%
2nd	22	60	20.6%	27	75	16.2%	59	163	2.3%	66	180	0.7%	73	200	0.4%

(Note: Case 3* corresponds to results using ASCE/SEI 7-16 method at MCE level.)

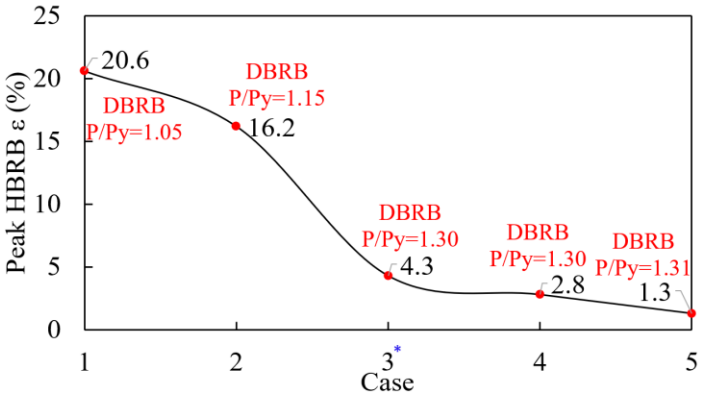


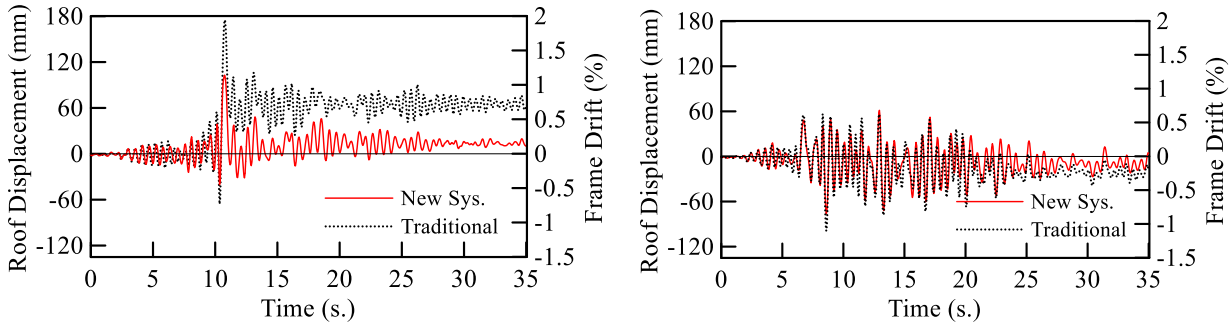
Figure 3. Peak HBRB strains vs. different cases of HBRB for NF6 motion.

Table 2. HBRB and DBRB properties and main results for all three floors (case 3* for NF6 motion).

Floor	HBRB Py (kN)	HBRB Asc (mm^2)	HBRB Max. Strain (%)	HBRB Max. P/Py	DBRB Max. Strain (%)	DBRB Max. P/Py
Roof	83	228	4.3%	1.34	0.44%	1.20
3rd	74	204	1.3%	1.23	0.75%	1.27
2nd	59	163	2.3%	1.31	0.94%	1.29

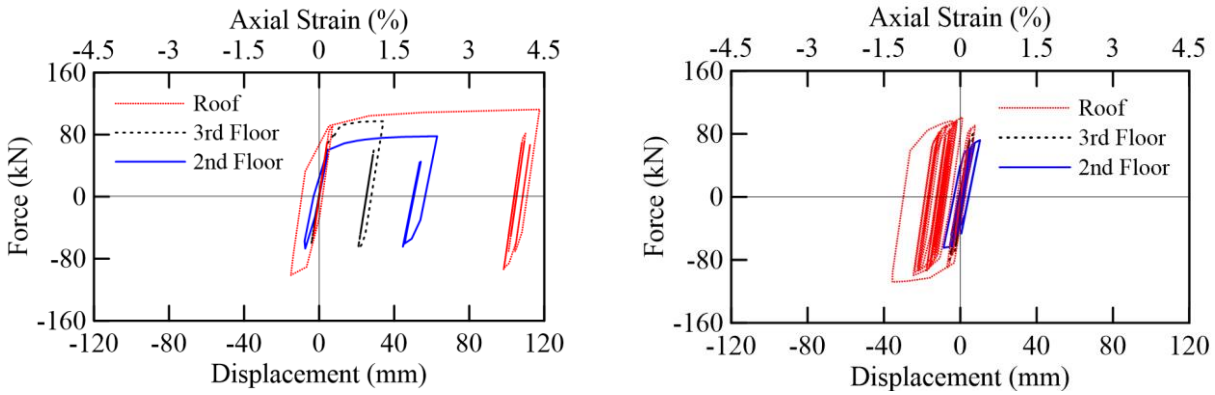
Fig. 4(a) shows the roof displacement response of both the traditional frame and new system (case 3*) under the strongest motion (NF6, Chi-Chi-TCU068). The maximum roof drift for the traditional and new system is 1.95% and 1.14%, respectively, and the corresponding maximum residual drift is 0.71% and 0.15%. Fig. 4(b) shows a similar plot for the frame under FF4 motion, where the peak roof drift for the traditional and new system is 1.10% and 0.85%, respectively, and the corresponding maximum residual drift is 0.19% and 0.05%. Fig. 5(a) and (b) shows the force-displacement response for HBRBs at all floors, showing larger energy dissipation at the roof. Fig. 6(a) and (b) shows the interstory displacement response of the slab at each floor, which can move with respect to the beam. For NF6 motion, the peak drifts are 3.5%, 1.2%, 3.7% and the residual drifts are 1.9%, 0.6% and 2.7% for the 2nd, 3rd and roof floors respectively. For FF4 motion, the peak drifts are 1.13%, 0.91%, 1.80% and the residual drifts are 0.09%, 0.11% and 0.39% for the 2nd, 3rd and roof floor respectively. Average peak interstory frame and slab drifts are plotted in Fig. 7 for the new system (case 3*) under 11 far-field and 11 near-fault motions. Traditional frame drifts are also plotted for comparison. In this figure, frame drifts are reduced by using the new system, thus reducing the frame ductility demand. However, the slab drift in the new system increases compared to the traditional frame system, indicating a possible tradeoff behavior (i.e., frame drift decreases while slab drift increases by allowing their relative movement). This observation is also shown in Fig. 6, where slab drifts, both peak and residual, are significant, particularly for NF6 motion.

Fig. 8 shows the force-displacement response of the first-story DBRB in both the traditional and new system under NF6 and FF4 motions. The new system shows a considerable reduction in the brace ductility demand, particularly for NF6 motion where the peak DBRB strain is reduced from 1.97 to 0.94% compared to the traditional frame system.



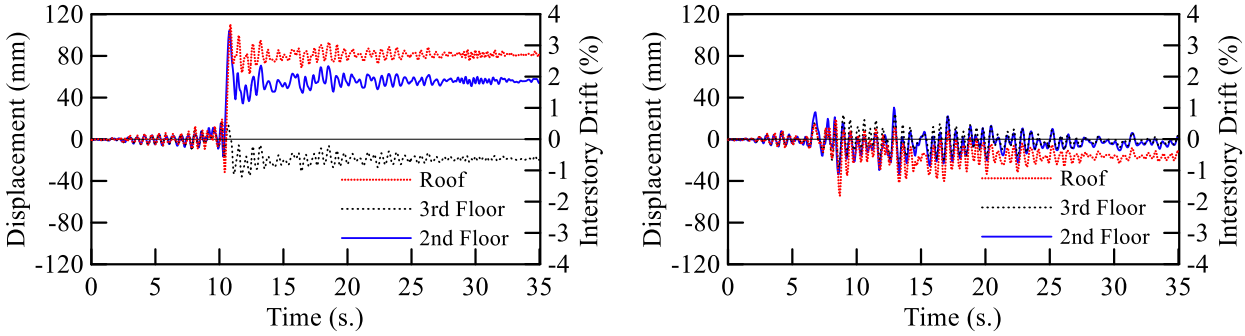
(a) NF6 motion. (b) FF4 motion.

Figure 4. Steel frame displacement response at roof level for the traditional and new system (case 3*)



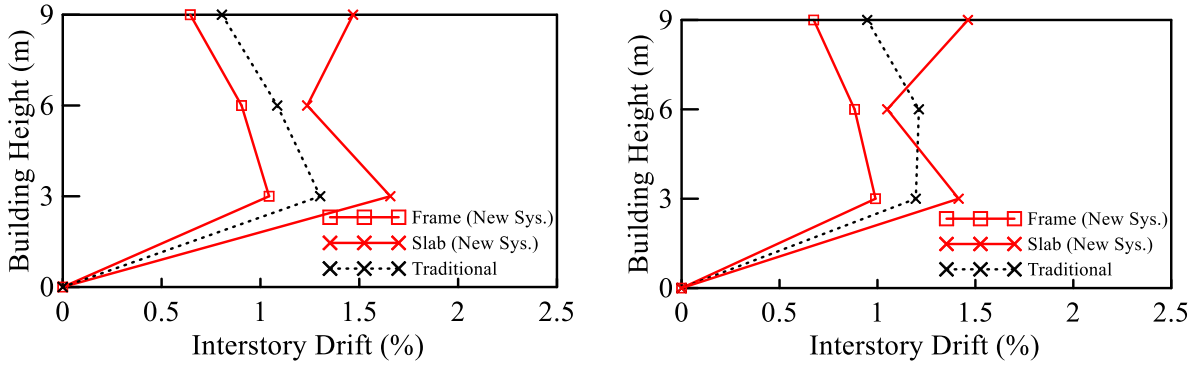
(a) NF6 motion. (b) FF4 motion

Figure 5. HBRB force vs. displacement response at all floors for NF6 and FF4 motions (case 3*)



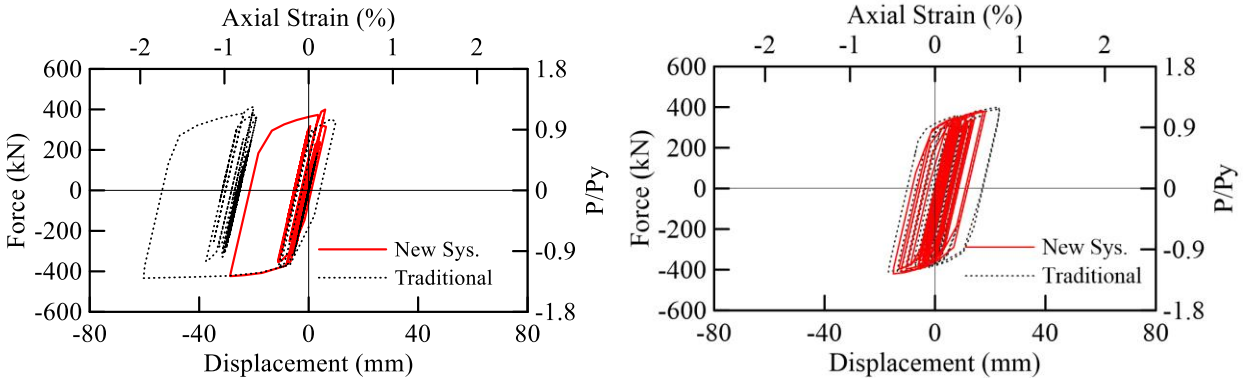
(a) NF6 motion. (b) FF4 motion.

Figure 6. Interstory slab displacement response at all floors for NF6 and FF4 motions (case 3*)



(a) Near-fault motions. (b) Far-field motions.

Figure 7. Average maximum drifts along building height for the traditional and new system (case 3*).



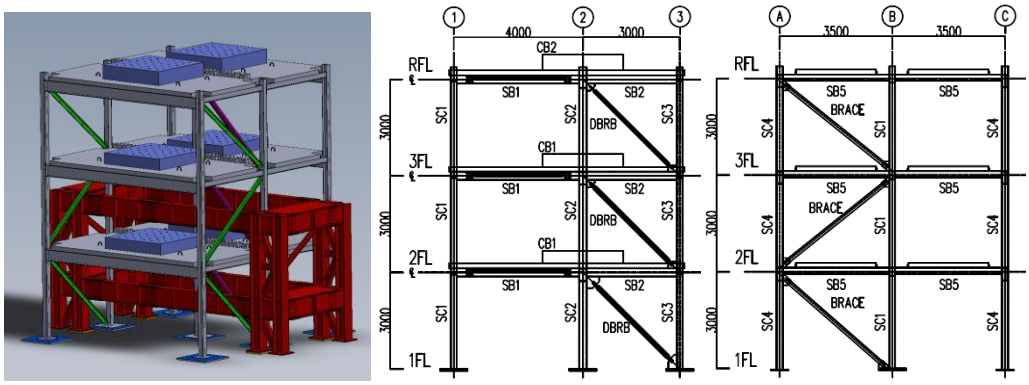
(a) NF6 motion. (b) FF4 motion.

Figure 8. First floor DBRB response for both the traditional and new system (case 3*)

SHAKE TABLE TESTS FOR A THREE-STORY FRAME

A full-scale, three-story prototype frame with a sliding concrete slab was designed and planned for shake table tests in Tainan laboratory. Fig. 9(a) shows the three-dimensional view of the specimen, Fig. 9(b) is the elevation view of B line and Fig. 9(c) is the elevation view of Lines 1 and 3. The B Line frame represents the Lateral Force Resisting System (LFRS), which is composed of a Special Moment Frame (SMF) on the left-hand side bay and a BRBF on the right-hand side bay. The Gravity Load Resisting System (GLRS) is located in the perimeter of the 3D frame and designed with pin connections for members. After adding concrete blocks, there are around 330 kN at 2FL and 3FL, and 350 kN at the roof. The total weight of the specimen is around 1000 kN. The P/P_y from columns SC1 to SC3 are 5.72%, 11.92% and 3.34% respectively.

Table 3 shows the section of each member. The width-to-thickness ratios (b/t) of box columns are 20.5 and 21.1, respectively, which are between the highly ductile member (b/t = 15.4) and moderately ductile (b/t = 28) member requirement in AISC 341-16 (2016). These similar box columns showed good response up to 4% drift in static cyclic loading based on previous isolated column or subassemblage tests (Chou and Chen 2020, Chou et al. 2022).



(a) 3D view (b) Line B (c) Lines 1 and 3

Figure 9. Full scale three-story steel frame specimen for shake table test (unit: mm)

Two test phases are planned to be conducted on the three-story dual frame system. In phase one, the frame with a precast sliding slab at each floor will be tested by using one of the motion in Fig. 2. Teflon pads will be placed between the slab and steel beams to reduce the interface friction force. These slabs connected to the steel beams in the LFRS through HBRBs are allowed to slide with respect to the frame in horizontal earthquake loading. Since the steel frame is expected to deform less than 1% drift (Fig. 7), the same frame will be tested in the second phase to investigate the seismic behavior of moderately ductile columns in the traditional dual system. To investigate the seismic behavior of the box columns in the dual system, the HBRB at each floor will be replaced by a structural T member designed to simulate a rigid connection between the slab and beams.

To minimize the out of plane movement of the sliding slabs during the test, vertical steel pads are positioned on the top of the beam flange on the periphery of the slab (see Fig. 10). A wide flange member as shown in Fig. 11(a) is fixed to the slab to provide lateral support to the steel beam at each floor in SMF and BRBF bays. Moreover, a slab at each floor is composed of two slabs bolted together as a unit [Fig. 11(b)].

Table 3. Member Section in Three-Story Frame

Type	Label	Section (mm)
Column	SC1, SC3	BOX 185x185x8
	SC2	BOX 225x225x10
	SC4	H 200x200x8x12
Beam	SB1, SB2	H 257x102x6x9
	SB3, SB4	H 400x200x8x13
	SB5	H 200x100x5.5x8
Type	Story	Section (mm)
BRACE	1F, 2F, 3F	DL 130x130x12
Structural T	1F, 2F, 3F	CT 145x200x8x13
Type	Place	Core area (mm^2)
DBRB	1F, 2F	900
	3F	400
HBRB	1F	162
	2F	204
	3F	228

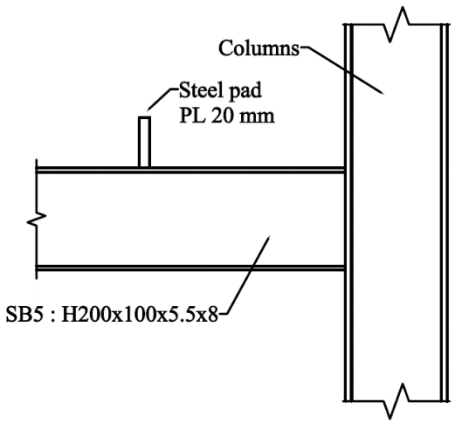
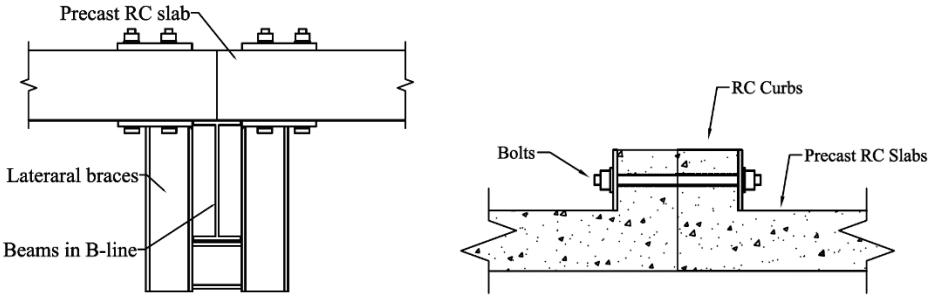


Figure 10. Steel pads to avoid rotation and lateral displacement of slab



(a) Lateral bracing setup (b) Bolted connection between precast slabs

Figure 11. Beam lateral braces and slab connection

CONCLUSIONS

This paper presents preliminary time analysis results for a three-story steel dual frame with a sliding slab at each floor, designed to reduce the seismic lateral force demand to the earthquake-resisting frame during earthquake motion. The HBRBs that are used to connect the sliding slab and the Lateral Force Resisting System (LFRS) were detemined based on the diaphragm design method in ASCE/SEI 7-16, 12.10.1 (2016), considering the maximum considered earthquake (MCE) force level. The design procedure limited the axial strain of HBRBs below 4.5% under 22 motions, scaled to the MCE level. The new system showed a considerable reduction in terms of the maximum frame drifts; however, its slab interstory drift was larger than that in the traditional dual frame. A shake table test will be conducted on the full-scale, three-story frame in Novemebr 2022 to validate the design procedure and the seimic response with either a sliding slab or rigidly-connected slab in earthquake motions.

ACKNOWLEDGEMENTS

This work is funded by the National Science and Technology Council under the project number MOST 111-2625-M-002-006, Taiwan and the 2022 Innovative Project of National Applied Research Laboratories.

REFERENCES

ASCE/SEI 7-16. Minimum design loads and associated criteria for buildings and other structures. American Society of Civil Engineers. 2016

Chopra, A. K., Newmark, N. M. (1980). Analysis, Chapter 2 in Design of Earthquake Resistant Structures. *ed. E. Rosenblueth, Pentech Press Ltd., London*.

Chou, C. C., Lai, Y. C., Xiong, H. C., Lin, T. H., Uang, C. M., Mosqueda G., Ozkula, G., El-Tawil, S., McCormick, J.P. (2022). "Effect of Boundary Condition on the Cyclic Response of I-Shaped Steel Columns: Two-Story Subassemblage versus Isolated Column Tests," *Earthquake Engineering and Structural Dynamics*, DOI: 10.1002/eqe.3730.

Chou, C. C., Xiong H. C., Kumar A., Lai Y. C., Uang, C. M. (2022). "Test and Finite Element Analysis of Two-Story Steel Subassemblage Frames with Highly and Moderately Ductile Box Columns", *8th Asia Conference on Earthquake Engineering*, Taipei, Taiwan.

Chou, C. C., Chen, G. W. (2020). "Lateral Cyclic Testing and Backbone Curve Development of High-Strength Steel Built-Up Box Columns Under Axial Compression. *Engineering Structures* 223, 111147

Chou, C. C., Chung, P. T., Cheng, Y. T. (2016). "Experimental Evaluation of Large-Scale Dual-Core Self-Centering Braces and Sandwiched Buckling-Restrained Braces." *Engineering Structures*, 116, 12-25.

Chou, C. C., Liu, J. H., Pham D. H. (2012). "Steel Buckling-Restrained Braced Frames with Single and Dual Corner Gusset Connections: Seismic Tests and Analyses." *Earthquake Engineering and Structural Dynamics,* 7(41): 1137-1156.

Chou, C. C., Chen, S. Y. (2010). "Subassemblage Tests and Finite Element Analyses of Sandwiched Buckling-restrained Braces." *Engineering Structures*, 32, 2108-2121.

Ghosh, S. K. (2016). Alternative diaphragm seismic design force level of ASCE 7-16. *Structure magazine*, 18-22.

Lin, T. H., Chou, C. C. (2022). "High-Strength Steel Deep H-Shaped and Box Columns under Proposed Near-Fault and Post-Earthquake Loadings." *Thin-Walled Structures*, 172, 108892

Lopez, O. A., Cruz, M. (1996). Number of modes for the seismic design of buildings. *Earthquake engineering & structural dynamics*, *25*(8), 837-855.

Tsampras, Georgios. "Force-Limiting Floor Diaphragm Connection for Earthquake-Resistant Buildings." PhD, Lehigh University, 2016. https://preserve.lehigh.edu/etd/2851.

Tsampras, G., Sause, R., Zhang, D., Fleischman, R. B., Restrepo, J. I., Mar, D., & Maffei, J. (2016). Development of deformable connection for earthquake-resistant buildings to reduce floor accelerations and force responses. *Earthquake Engineering & Structural Dynamics*, *45*(9), 1473-1494.

Tsampras, G., Sause, R. (2022). Force-Based Design Method for Force-Limiting Deformable Connections in Earthquake-Resistant Buildings. *Journal of Structural Engineering*, *148*(10), 04022150.

Tsampras G., Sause R., Fleischman R. B., Restrepo J. I., Nema A., Zhang Z., Practical force-limiting deformable connections in buildings with rocking base mechanism and limited higher-mode responses. *Proceedings of the 12th National Conference in Earthquake Engineering*, Earthquake Engineering Research Institute, Salt Lake City, UT. 2022.

Zhang, Z., Fleischman, R. B., Restrepo, J. I., Guerrini, G., Nema, A., Zhang, D., Ulina, S., Tsampras, G., Sause, R., (2018). Shake-table test performance of an inertial force-limiting floor anchorage system. *Earthquake Engineering & Structural Dynamics*, *47*(10), 1987-2011.